Research Square

Preprints are preliminary reports that have not undergone peer review.
They should not be considered conclusive, used to inform clinical practice,
or referenced by the media as validated information.

Terahertz imaging resolves ice porosity at the millimetre scale

Linus Leo Stöckli

linus.stoeckli@unibe.ch

Space Research and Planetary Sciences, Physics Institute, University of Bern, Bern, Switzerland.

Rafael Ottersberg

Space Research and Planetary Sciences, Physics Institute, University of Bern, Bern, Switzerland.

Antoine Pommerol

Space Research and Planetary Sciences, Physics Institute, University of Bern, Bern, Switzerland.

Dominik Belousov

Space Research and Planetary Sciences, Physics Institute, University of Bern, Bern, Switzerland.

Nicolas Thomas

Space Research and Planetary Sciences, Physics Institute, University of Bern, Bern, Switzerland.

Article

Keywords:

Posted Date: November 11th, 2026

DOI: https://doi.org/10.21203/rs.3.rs-11143371/v1

License: This work is licensed under a Creative Commons Attribution 4.0 International License.
Read Full License

Additional Declarations: No competing interests reported.

Terahertz imaging resolves ice porosity at the millimetre scale

Linus Leo Stöckli[1*], Rafael Ottersberg[1], Antoine Pommerol[1], Dominik Belousov[1], Nicolas Thomas[1]

[1*]Space Research & Planetary Science Division, University of Bern, Sidlerstrasse 5, Bern, 3012, Bern, Switzerland.

*Corresponding author(s). E-mail(s): linus.stoeckli@unibe.ch;
Contributing authors: rafael.ottersberg@unibe.ch;
antoine.pommerol@unibe.ch; dominik.belousov@unibe.ch;
nicolas.thomas@unibe.ch;

Abstract

The porosity and small-scale structure of ice and snow influence their physical properties and provide information about the processes that form and modify icy surfaces. However, existing in-situ methods for measuring ice porosity are generally either destructive or unable to resolve spatial variations at the millimetre scale. Here we show that terahertz time-domain spectroscopy (THz-TDS) enables non-destructive, spatially resolved measurements of ice porosity. We measure the complex refractive index of porous ice samples and retrieve porosity using effective-medium theory, producing two-dimensional maps of thickness-averaged apparent porosity with sub-millimetre spatial resolution and centimetre-scale penetration. Against gravimetric porosity measurements, a Bruggeman effective-medium inversion retrieves porosity with a root-mean-square error of 5.7 % and a systematic underestimation of 4.8 %. Measurements under both atmospheric and vacuum conditions demonstrate the applicability of the approach across different environmental conditions. These results establish THz-TDS as a non-destructive method for resolving small-scale variations in ice porosity, with potential applications in terrestrial cryospheric field measurements and the in-situ exploration of icy planetary surfaces.

Keywords: THz Time Domain Spectroscopy, Ice, Porosity, Density, Volume Fraction

1 Introduction

Measuring the porosity of ice and snow is crucial for understanding the deposition and evolution of ice on planetary bodies, as well as the physical properties and evolution of Earth's cryosphere. For example, in cometary research, surface porosity can influence cometary activity by controlling local thermal contact and, consequently, heat transport through the near-surface material (Seiferlin, Spohn, & Benkhoff, 1995) or in avalanche risk assessment where the stress concentration is linked to snow porosity/density (Gaume, Chambon, Herwijnen, & Schweizer, 2018; Wautier, Geindreau, & Flin, 2015). Currently, porosity of samples can be accurately measured in the laboratory using a X-ray Computer Tomograph (XCT) (Coléou, Lesaffre, Brzoska, Ludwig, & Boller, 2001). Although, in the field, ice and snow density or porosity can be measured with established methods such as various density cutters (Proksch, Rutter, Fierz, & Schneebeli, 2016) or the snow micro pen (SMP) (Johnson & Schneebeli, 1999; Marshall, Schneebeli, & Koh, 2007; Van Herwijnen, 2013), these methods offer limited spatial resolution of the sample and face additional challenges when applied to thick, dense ice layers (Krampe, Kauker, Dumont, & Herber, 2023). While the "Finnish Snow Fork" is also a non-destructive instrument, it operates at around 1 GHz and thus has limited spatial resolution and cannot resolve the local structure of a sample (Sihvola & Tiuri, 1986). Even more so, Ground Penetrating Radar (GPR) can be used to obtain a global estimate of a large area (Bonnell et al., 2023; Kovacs, Gow, & Morey, 1995; Zhao, Forte, Colucci, & Pipan, 2016) in the field, but a local measurement of a small area is hindered by the diffraction limit at radar wavelengths. To mitigate this, we need to move to shorter wavelengths. Effective Medium Theory (EMT) can be used to calculate the effective permittivity $\tilde{\varepsilon}_{\text{eff}}$ of a mixture of components. If we set one component to vacuum ($\tilde{\varepsilon}_{\text{vacuum}} = 1$) and the other to ice, we can reverse this to determine the porosity from the effective permittivity measurement. For example, Bossa et al. (2015) used EMT in the mid-infrared to determine porosity and volumetric fraction of ice mixtures. Further, Bossa et al. (2014) have used EMT and an FTIR (Fourier Transform Infrared) spectrometer to measure a narrow range of porosities (0.2 - 0.3) of astrophysical CO_2 and H_2O ice mixtures with a 632.8 nm laser using EMT. Similarly, Millán, Luna, Domingo, Satorre, and Santonja (2025); Millán, Santonja, Domingo, Luna, and Satorre (2019) studied the porosities of astrophysical ices, for example CO_2. Their samples had thicknesses up to 1 µm. Although visible light can penetrate water ice, strong scattering within the ice limits the achievable spatial resolution. THz frequencies are located at the sweet-spot of the spectrum, where we still have adequate penetration depth (centimetre scale) but also a spatial resolution at the millimetre scale. Gavdush et al. (2026) determined the spectroscopic properties of porous and solid lh, lc and amorphous H_2O ice samples in the THz-IR range. We are specifically interested in THz-TDS (Terahertz Time Domain Spectroscopy) which has been shown to be able to produce attenuation images in order to determine the porosity of rocks (Bouchard, Eichmann, Ow, Poitzsch, & Petkie, 2022) or cement (Tian et al., 2026) and to compare low density amorphous ice (LDA) and high density amorphous ice (HDA) ice samples (Häßner, Mutschke, Blum, Zeller, & Gundlach, 2018). Stöckli et al. (n.d.) have shown that THz-TDS can be used to extract sub-surface ice

pebbles in cometary analogues. In this work, we present the application of THz-TDS to extract the local porosity and structure of ice samples.

2 Results

Figure 1 shows the residuals of the estimated values using EMT. Each measurement was taken with the collimated beam setup with a FWHM of $\approx 12\,\mathrm{mm}$ and averaged over 1000 measurements. All measurements were taken under vacuum, except for dataset 6, which was taken at ambient pressure. All measurements of the vacuum samples and references were taken at temperatures below 175 K and pressures below 1×10^{-1} mbar. Samples in datasets 1 and 2 are composed of SPIPA-B spherical ice particles (Pommerol et al., 2019), all samples with higher porosity are composed of frost. Samples with low porosity (< 0.1) are solid ice slabs.

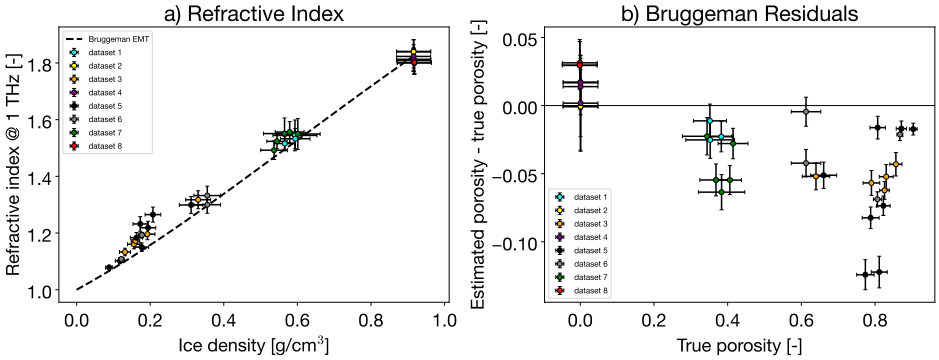


Fig. 1: Refractive index measurements (a) and porosity residuals (b) for the Bruggeman EMT model.

Across 25 porous samples in Figure 1, Bruggeman-derived porosity underestimated gravimetric porosity by 4.8 % on average, with a residual scatter of 3.1 % and an RMSE of 5.7 %.

THz time domain spectroscopy can also be used to spatially resolve the porosity of ice samples. We switched the setup from the collimated beam to a focused beam with a FWHM of $\approx 1.5\,\mathrm{mm}$. The samples were then scanned in a meander pattern with pixel sizes of $0.5\,\mathrm{mm} \times 0.5\,\mathrm{mm}$. The raw datasets were inspected using THz Image Explorer (Stöckli, Demion, & Thomas, 2025). Then Bruggeman EMT was used to convert the refractive index into porosity values for each pixel, as shown in Figure 2.

We have averaged the porosity of sectors A, B, C and D and compared it to the true porosity obtained from sample preparation in Table 1.

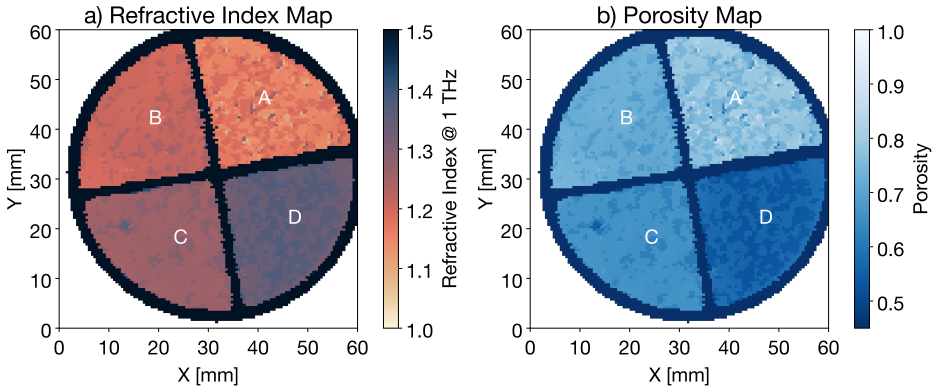


Fig. 2: 2D THz image of four sectors of 10 mm thick samples with different porosities. The diameter of the sample holder is 60 mm. This image was acquired with the focused THz setup with a FWHM of $\approx$ 1.5 mm, yielding a spatial resolution of 1 mm. The calculated refractive index is shown in a) and the extracted porosity using Bruggeman EMT in b).

sector	**True Porosity** [-]	**Estimated Porosity** [-]
A	0.78 ± 0.05	0.77 ± 0.04
B	0.69 ± 0.05	0.72 ± 0.02
C	0.60 ± 0.05	0.65 ± 0.02
D	0.51 ± 0.05	0.55 ± 0.02

Table 1: Extracted porosity compared to the true porosity of each of the different sectors. The error values of the estimated porosities are obtained from averaging the different sectors.

3 Methods

3.1 THz Time Domain Spectroscopy

THz time domain spectroscopy (THz-TDS) closes the THz-gap between the infrared (IR) and microwave regimes, offering observations underneath the surface at centimetre scale depths and millimetre scale spatial resolution. Furthermore, THz-TDS records the transmitted or reflected pulse in the time domain, thereby obtaining the amplitude and phase information. Hence, this allows the extraction of optical properties such as absorption coefficient and refractive index. Measurements were acquired with the COCoNuT setup (Stöckli, Brändli, et al., 2025) which is based on the Toptica TeraFlash Pro spectrometer. The setup has been adapted such that the sample can be placed in a collimated beam with a FWHM of $\approx$ 12 mm. This reduces artifacts as the THz pulse travels through a thick sample and averages out local inhomogeneities. To measure the refractive index, the signal from a single pixel at the center of the sample

holder was averaged 1000 times. To acquire an image, the whole sample holder was scanned using the meander strategy and a focused beam with a FWHM of $\approx 1.5\,\mathrm{mm}$, the single pixels are not averaged.

3.2 Effective Medium Theory

Effective Medium Theory (EMT) is usually used to determine the refractive index and absorption coefficients of the materials embedded in a matrix material with known properties. The Bruggeman equation (Markel, 2016) is based on the mean field approximation, assumes mostly spherical particles and is symmetrical, meaning it does not strictly assume a host material. It is given in Equation 1.

$$\mathbf{v}_h \frac{\tilde{\varepsilon}_h(\omega) - \tilde{\varepsilon}_{\mathrm{eff}}(\omega)}{\tilde{\varepsilon}_h(\omega) + 2\,\tilde{\varepsilon}_{\mathrm{eff}}(\omega)} = -\sum_{i=1}^{n} \mathbf{v}_i \frac{\tilde{\varepsilon}_i(\omega) - \tilde{\varepsilon}_{\mathrm{eff}}(\omega)}{\tilde{\varepsilon}_i(\omega) + 2\,\tilde{\varepsilon}_{\mathrm{eff}}(\omega)}, \tag{1}$$

We now reduce Equation 1 to a binary mixture of ice and vacuum, setting $\tilde{\varepsilon}_h = \tilde{\varepsilon}_{\mathrm{vacuum}} = 1$. We can then insert the measured permittivity $\tilde{\varepsilon}_i$ at 1 THz (mean value of the range 0.9 THz - 1.1 THz) and the effective permittivity of solid ice (Tao et al. (2024) and section A) $\tilde{\varepsilon}_{\mathrm{eff}}$ and solve for the volumetric ratio $\mathbf{v}_i$. For a binary mixture, it follows that

$$\mathbf{v}_h = 1 - \mathbf{v}_i.$$

The complex refractive indices of the individual samples were determined using Equation 2 - Equation 4 (Leung, Ward-Berry, Wanvig I Dot, Lee, & Zeitler, 2025) and a reference measurement of the silicon window of the empty sample holder $n_{\mathrm{ref}}(f)$. The reference measurement was repeated for each measurement campaign to correct for internal temporal shifts in the instrument.

$$n(f) = n_{\mathrm{ref}}(f) + \frac{c\Delta\phi(f)}{2\,\pi f d} \tag{2}$$

$$\alpha(f) = -\frac{2}{d} \ln\left(\frac{E_{\mathrm{sample}}(f)}{E_{\mathrm{ref}}(f)} \frac{(n(f) + n_{\mathrm{ref}}(f))^2}{4\,n(f)\,n_{\mathrm{ref}}(f)} \right) = \frac{4\,\pi f k(f)}{c} \tag{3}$$

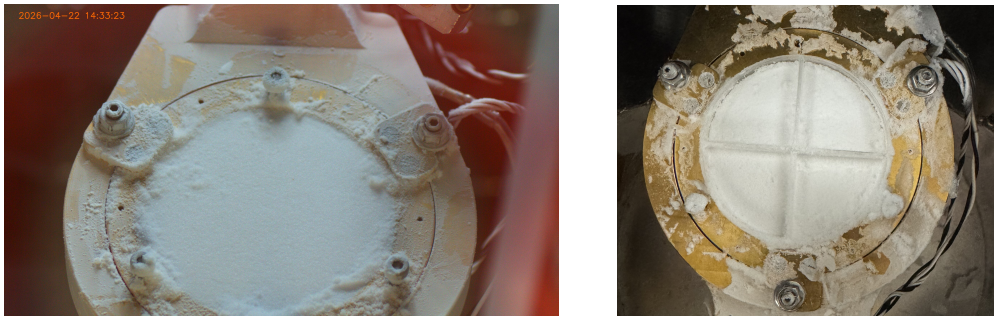
$$\tilde{n} = n - i\,k = \sqrt{\tilde{\varepsilon}} \tag{4}$$

Where $\Delta\phi(f) = \phi_{\mathrm{ref}}(f) - \phi_{\mathrm{sample}}(f)$ is the phase difference obtained from the FFT, d is the thickness of the sample and c is the speed of light.

3.3 Sample Preparation

Solid ice was obtained by slowly freezing liquid water at ambient pressure and then preparing the top surface to be flat and parallel. Medium density snow was obtained by producing SPIPA-B (with a mean diameter of 67 µm and a porosity of 49.3 %) (Pommerol et al., 2019). Low density snow was obtained with the Frost Collection Tower (FCT), described in section B, and has an average density of $0.1\,\mathrm{g\,cm^{-3}}$, which roughly equals a porosity of 90 %.

The sample was collected and sieved through a 1 mm sieve and was then placed in a sample holder with 60 mm diameter and a height of 10 mm. Low density samples were loosely placed in the sample holder and the top surface was flattened. For more dense samples, a larger amount was placed in the pre-cooled sample holder and compressed to 10 mm, 7.5 mm or 5 mm with precise tampers as shown in Figure 3. The density of the samples was determined after preparation by measuring the mass of the full sample holder, thus yielding the gravimetric porosity of the sample.



(a) SPIPA-B (b) Frost

Fig. 3: Porous SPIPA-B ice with a density of $0.56\,\mathrm{g\,cm^{-3}}$ in the 60 mm diameter sample holder with a flat surface tamped to 10 mm thickness (a) and the COC four sector sample holder filled with different amounts of frost and tamped to 10 mm (b).

To image multiple porosities at once, a 3D printed sample holder with four sectors made from cyclic olefin copolymer (COC) was used. COC is known for its low outgassing in vacuum and high transparency at THz frequencies. Each sector was filled with different amounts of frost and then compressed to 10 mm. To measure the effective permittivity of solid ice, water was poured in the sample holder and slowly frozen at ambient pressure. After it transitioned completely to ice, the surface was flattened by pressing a warm metal piston on top. After preparing the surface, the sample was placed in vacuo.

4 Discussion

The results appear to be very good but were made under ideal conditions. The following points should be noted. All measurements were obtained with a planar surface. Rough surfaces at the millimetre scale will likely introduce scattering and variations in thickness, thus less accurate results. The error-bars originate from the thickness and mass measurements. The mass is only used to determine the actual porosity whereas the thickness is also required to calculate the refractive index. Since the gravimetric porosity and the estimated porosity both depend on the uncertainty of the thickness measurements, the covariance had to be taken into account when calculating the errors on the residuals, resulting in smaller error bars. Measuring the true porosity

with a different method like a micro-CT would lead to a more accurate comparison. In Figure 1 we see that the refractive index of the measurements is higher than what the Bruggeman EMT predicts. It is likely that the samples are not uniform in density, and more dense in the center where it was probed with the THz beam. This is an artifact of the sample preparation. We suspect that the spread of the data is caused by sublimation when the sample is introduced in the vacuum chamber, this is especially noticeable for highly porous samples where the thermal contact to the cold sample holder is poor and the surface of the ice is thus much warmer. A misalignment of the sample holder and/or optical path of the THz beam can also introduce errors. Bruggeman EMT approximates individual particles as spheres, which certainly breaks for the irregular frost samples, thus in future work it should be investigated if the relation of the refractive index and porosity can be improved with a different model. While most measurements were taken under vacuum conditions because the ice samples are preserved longer at low pressures, our experiments have shown that it is entirely possible to measure the refractive index equally accurately at ambient pressure as long as the ice sample remains stable. Continuously scanning an ice sample and measuring the porosity while it is warming up can potentially be used to observe sublimation processes.

5 Conclusion

We have shown that THz-TDS can be used to determine the porosity of snow or icy samples under atmospheric or vacuum conditions. Bruggeman underestimates porosity by an average of 4.8 %, with approximately 3.1 % of residual scatter around this bias. We expect the accuracy to be higher if a more precise porosity reference is used. We are confident that this work shows the possibility of future implementations of a THz instrument to measure the local porosity/density of ice samples in field campaigns on Earth or in-situ space missions to planetary bodies like comets, Mars or icy-moons such as Enceladus. Implementations with narrow/focused beams and imaging systems could provide more information about the local ice-structure and inhomogeneities.

Acknowledgements. This work was supported through a MARVIS (Multidisciplinary Advanced Research Ventures in Space) programme of the Swiss State Secretariat for Education, Research and Innovation (SERI) called SUBICE. SUBICE is a project of the University of Bern (UniBe), the University of Applied Sciences and Arts, Western Switzerland (HES-SO), and Thales-Alenia Space Switzerland (TASCH). The authors want to thank the Space Research & Planetary Sciences fine mechanical and electronics departments, specifically: Mathias Brändli, Daniele Piazza, Sébastien Hayoz, Iljadin Manurung, Harald Mischler and Claudio Zimmermann for their help with the laboratory setup.

Declarations

The authors declare that there is no conflict of interest.

Data Availability

The raw data as well as all plots with the corresponding datapoints in CSV files are also available on zenodo: https://doi.org/10.5281/zenodo.22863554.

Code Availability

The reproducible capsule with the code and raw data is available on Code Ocean under https://doi.org/10.24433/CO.2223647.v1.

Funding

This work was funded through a MARVIS (Multidisciplinary Advanced Research Ventures in Space) programme of the Swiss State Secretariat for Education, Research and Innovation (SERI) called SUBICE. SUBICE is a project of the University of Bern (UniBe), the University of Applied Sciences and Arts, Western Switzerland (HES-SO), and Thales-Alenia Space Switzerland (TASCH). The contribution of RO and AP has been carried out within the framework of the NCCR PlanetS supported by the Swiss National Science Foundation under grants 51NF40-182901 and 51NF40-205606.

Author Contributions

L. L. Stöckli conceived the idea for the study, performed the sample preparation, data acquisition and data analysis. R. Ottersberg, A. Pommerol, D. Belousov and N. Thomas contributed to the sample preparation and data analysis techniques. N. Thomas was responsible for securing the financial support. All co-authors commented on the manuscript and provided input to its final version.

Appendix A Solid ice refractive index

The measurements, displayed in Figure A1, of the refractive index of solid ice agree well with literature (Tao et al., 2024) around 1 THz, see Figure A1. Tao et al. (2024) themselves noticed slight deviations between different THz spectrometers. We observe a sign change of the slope below 1.6 THz which was also reported by Tao et al. (2024).

Appendix B Frost Collection Tower

The FCT consists of a brass tube with a diameter of 55 mm and a height of 300 mm. The tube was submerged in a container filled with liquid nitrogen as shown in Figure B2. Frost slowly starts to deposit on the upper part of the tube and can be scraped off every 10 minutes. The frost then falls in the liquid nitrogen and is conserved.

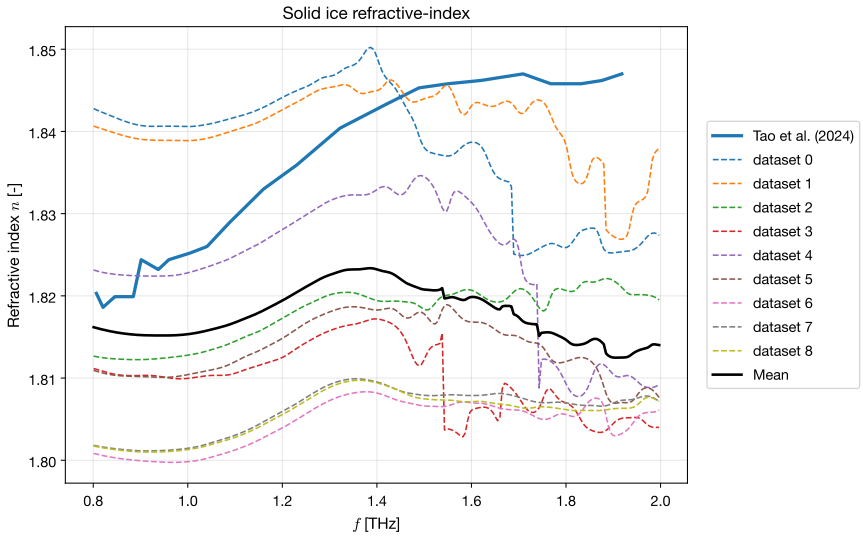


Fig. A1: Refractive index of solid ice compared to literature. We hit the noise floor after 1.6 THz.

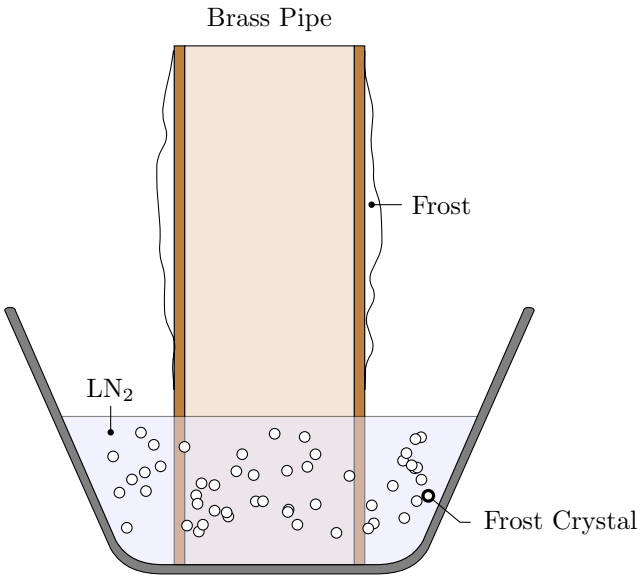


Fig. B2: The Frost Collection Tower (FCT) consists of a brass pipe placed in liquid nitrogen (LN_2). The humidity in the ambient air causes a frost build up on the cold surface of the pipe. This frost is then either scraped off or washed off by pouring liquid nitrogen over the brass pipe. The frost crystals are conserved in the liquid nitrogen.

References

Bonnell, R., McGrath, D., Hedrick, A.R., Trujillo, E., Meehan, T.G., Williams, K., ... Hale, K.E. (2023, October). Snowpack relative permittivity and density derived from near-coincident lidar and ground-penetrating radar. *Hydrological Processes*, *37*(10), e14996, https://doi.org/10.1002/hyp.14996

Bossa, J.-B., Isokoski, K., Paardekooper, D.M., Bonnin, M., Van Der Linden, E.P., Triemstra, T., ... Linnartz, H. (2014, January). Porosity measurements of interstellar ice mixtures using optical laser interference and extended effective medium approximations. *Astronomy & Astrophysics*, *561*, A136, https://doi.org/10.1051/0004-6361/201322549

Bossa, J.-B., Maté, B., Fransen, C., Cazaux, S., Pilling, S., Rocha, W.R.M., ... Linnartz, H. (2015, November). Porosity and band-strength measurements of multi-phase composite ices. *The Astrophysical Journal*, *814*(1), 47, https://doi.org/10.1088/0004-637X/814/1/47

Bouchard, J., Eichmann, S.L., Ow, H., Poitzsch, M., Petkie, D.T. (2022, October). Terahertz imaging for non-destructive porosity measurements of carbonate rocks. *Scientific Reports*, *12*(1), 18018, https://doi.org/10.1038/s41598-022-22535-z

Coléou, C., Lesaffre, B., Brzoska, J.-B., Ludwig, W., Boller, E. (2001). Three-dimensional snow images by X-ray microtomography. *Annals of Glaciology*, *32*, 75–81, https://doi.org/10.3189/172756401781819418

Gaume, J., Chambon, G., Herwijnen, A.V., Schweizer, J. (2018, August). Stress Concentrations in Weak Snowpack Layers and Conditions for Slab Avalanche Release. *Geophysical Research Letters*, *45*(16), 8363–8369, https://doi.org/10.1029/2018GL078900

Gavdush, A.A., Ribeiro, F., Matveishina, M.K., Vyjidak, A., Kruczkiewicz, F., Komandin, G.A., ... Caselli, P. (2026, June). Broadband spectroscopy of astrophysical ice analogues: V. Optical constants of Ih, Ic, and amorphous H_2O ices in the terahertz-infrared range. *Astronomy & Astrophysics*, *710*, A89, https://doi.org/10.1051/0004-6361/202659623

Häßner, D., Mutschke, H., Blum, J., Zeller, T., Gundlach, B. (2018, December). Laboratory measurements of the sub-millimetre opacity of amorphous and micro-particulate H2O ices for temperatures above 80 K. *Monthly Notices of the Royal*

Astronomical Society, *481*(4), 5022–5033, https://doi.org/10.1093/mnras/sty2664

Johnson, J.B., & Schneebeli, M. (1999, December). Characterizing the microstructural and micromechanical properties of snow. *Cold Regions Science and Technology*, *30*(1-3), 91–100, https://doi.org/10.1016/S0165-232X(99)00013-0

Kovacs, A., Gow, A.J., Morey, R.M. (1995, May). The in-situ dielectric constant of polar firn revisited. *Cold Regions Science and Technology*, *23*(3), 245–256, https://doi.org/10.1016/0165-232X(94)00016-Q

Krampe, D., Kauker, F., Dumont, M., Herber, A. (2023, May). Snow and meteorological conditions at Villum Research Station, Northeast Greenland: on the adequacy of using atmospheric reanalysis for detailed snow simulations. *Frontiers in Earth Science*, *11*, 1053918, https://doi.org/10.3389/feart.2023.1053918

Leung, C.K., Ward-Berry, J.N., Wanvig I Dot, E., Lee, J., Zeitler, J.A. (2025, September). Tutorial: Accurate Determination of Refractive Index and Absorption Coefficient in Terahertz Time-Domain Spectroscopy. *Journal of Infrared, Millimeter, and Terahertz Waves*, *46*(9), 59, https://doi.org/10.1007/s10762-025-01070-8

Markel, V.A. (2016, July). Introduction to the Maxwell Garnett approximation: tutorial. *Journal of the Optical Society of America A*, *33*(7), 1244, https://doi.org/10.1364/JOSAA.33.001244

Marshall, H.-P., Schneebeli, M., Koh, G. (2007, January). Snow stratigraphy measurements with high-frequency FMCW radar: Comparison with snow micropenetrometer. *Cold Regions Science and Technology*, *47*(1-2), 108–117, https://doi.org/10.1016/j.coldregions.2006.08.008

Millán, C., Luna, R., Domingo, M., Satorre, M., Santonja, C. (2025, November). Experimental and theoretical porosity determination for ices of astrophysical interest: CH4, C2H4, C2H6, CH3OH, N2, NH3, CO, and CO2. *Icarus*, *441*, 116710, https://doi.org/10.1016/j.icarus.2025.116710

Millán, C., Santonja, C., Domingo, M., Luna, R., Satorre, M.A. (2019, August). An experimental test for effective medium approximations (EMAs): Porosity determination for ices of astrophysical interest. *Astronomy & Astrophysics*, *628*,

A63, https://doi.org/10.1051/0004-6361/201935153

Pommerol, A., Jost, B., Poch, O., Yoldi, Z., Brouet, Y., Gracia-Berná, A., ... Thomas, N. (2019, August). Experimenting with Mixtures of Water Ice and Dust as Analogues for Icy Planetary Material: Recipes from the Ice Laboratory at the University of Bern. *Space Science Reviews*, *215*(5), 37, https://doi.org/10.1007/s11214-019-0603-0

Proksch, M., Rutter, N., Fierz, C., Schneebeli, M. (2016, February). Intercomparison of snow density measurements: bias, precision, and vertical resolution. *The Cryosphere*, *10*(1), 371–384, https://doi.org/10.5194/tc-10-371-2016

Seiferlin, K., Spohn, T., Benkhoff, J. (1995). Cometary ice texture and the thermal evolution of comets. *Advances in Space Research*, *15*(10), 35–38, https://doi.org/10.1016/0273-1177(94)00148-T

Sihvola, A., & Tiuri, M. (1986, September). Snow Fork for Field Determination of the Density and Wetness Profiles of a Snow Pack. *IEEE Transactions on Geoscience and Remote Sensing*, *GE-24*(5), 717–721, https://doi.org/10.1109/TGRS.1986.289619

Stöckli, L.L., Brändli, M., Piazza, D., Ottersberg, R., Pommerol, A., Murk, A., Thomas, N. (2025, March). Design and commissioning of a THz time-domain spectro-goniometer in a cryogenic comet simulation chamber. *Review of Scientific Instruments*, *96*(3), 034502, https://doi.org/10.1063/5.0252742

Stöckli, L.L., Demion, A., Thomas, N. (2025, November). THz Image Explorer - An Interactive Cross-Platform Open-Source THz Image Analysis Tool. *Journal of Open Source Software*, *10*(115), 8754, https://doi.org/10.21105/joss.08754

Stöckli, L.L., Hervé Girard, Rafael Ottersberg, Dominik Belousov, Arnaud Demion, Antoine Pommerol, ... Nicolas Thomas (n.d.). Resolving Sub-Surface Ice Pebbles in Cometary Simulants using THz Time-Domain Spectroscopy. *JGR: Planets*, , (in review)

Tao, Y.H., Dai, X., Moggach, S.A., Clode, P.L., Fitzgerald, A.J., Hodgetts, S.I., ... Wallace, V.P. (2024, June). The spectrum of Ih ice using terahertz time-domain spectroscopy. *The Journal of Chemical Physics*, *160*(21), 214503, https://doi.org/10.1063/5.0193458

Tian, L., Wang, Z., Chen, Y., Zhang, W., Wang, L., Li, X. (2026, June). Terahertz Time-Domain Spectroscopy for Non-Contact Porosity Estimation and Hydration Assessment of Hardened Cement Paste. *Materials*, *19*(13), 2726, https://doi.org/10.3390/ma19132726

Van Herwijnen, A. (2013, October). Experimental analysis of snow micropenetrometer (SMP) cone penetration in homogeneous snow layers. *Canadian Geotechnical Journal*, *50*(10), 1044–1054, https://doi.org/10.1139/cgj-2012-0336

Wautier, A., Geindreau, C., Flin, F. (2015, October). Linking snow microstructure to its macroscopic elastic stiffness tensor: A numerical homogenization method and its application to 3-D images from X-ray tomography. *Geophysical Research Letters*, *42*(19), 8031–8041, https://doi.org/10.1002/2015GL065227

Zhao, W., Forte, E., Colucci, R.R., Pipan, M. (2016, August). High-resolution glacier imaging and characterization by means of GPR attribute analysis. *Geophysical Journal International*, *206*(2), 1366–1374, https://doi.org/10.1093/gji/ggw208